

Three-dimensional Bi₂WO₆/graphene aerogel electrode for high-performance supercapacitor

Xun Xu, Fangwang Ming, Jinqing Hong, Zhoucheng Wang*

Biochemical Engineering, College of Chemistry and Chemical Engineering, Xiamen University, 422 Siming South Road, Xiamen, 361000, China

*Corresponding author

DOI: 10.5185/amlett.2018.1719

www.vbripress.com/aml

Abstract

Graphene-based aerogels with porous structure and three-dimensional (3D) network have attracted plentiful interests recently because they could exhibit as an excellent matrix for various kinds of nanoparticles, thus providing a potential prospect in a variety of applications. In this report, 3D composite aerogel with poriferous structure assembly of bismuth tungstate sheets and graphene nanosheets has been prepared by a simple hydrothermal process. The 3D multihole structure of the hybrid aerogel could not only provide enormous surface area, but also facilitate electron transfer and ion transmission which could decrease the electrode internal resistance and consequently improve the capacitive property. As a result, the Bi₂WO₆/graphene hybrid aerogel achieves a large specific capacitance of 714 F g⁻¹ at the current density of 4 A g⁻¹. The hybrid aerogel could provide a new method for developing high-performance energy storage materials. Copyright © 2018 VBRI Press.

Keywords: Graphene, hydrothermal synthesis, aerogel, porous materials, supercapacitor.

Introduction

Developing renewable and sustainable energy conversion and storage technology have stimulated a large of research for worldwide researchers due to the rapidly increasing modern energy consumption. Electrochemical devices such as photovoltaic solar cells, supercapacitors, lithium ion batteries, and hydrogen cells are mainly renewable energy storage systems [1-5]. Among them, supercapacitors have been attracting a lot of attentions due to their high power densities, fast rates of charge-discharge, long cycle life and service life, safe operation and environmental friendliness [5-7]. However the volumetric capacitance of commercial activated carbon electrodes are at around 60 F cm⁻³ for supercapacitors, and about 320 F cm⁻³ for low-density foam carbons at best [8-9]. Notwithstanding, the energy density of traditional carbon-based capacitors is too low to meet the actual requirements [5-9]. Therefore, in order to take place of fossil fuel, it is important to further increase the energy density of present supercapacitors. Recently, Bismuth-based compounds such as bismuth vanadate [10], bismuth oxide [11], bismuth tungstate and bismuth sulfide [12, 13] have been investigated for energy storage materials. Among them, bismuth tungstate could be a better candidate as a result of its stableness, excellent anions conducting, and good non-linear dielectric susceptibility [12, 13]. However, the electroconductibility of the Bismuth-based compounds are still too low to support rapid electron transfer during the work [10-13].

Graphene aerogel (GA) is a three-dimensional (3D) poriferous architecture and conductive framework constructed with graphene [14]. The large specific area, excellent conductivity and highly porosity makes GA as an excellent matrix for energy storage devices [14, 15]. Although, Bi₂WO₆/graphene composite aerogel has already been synthesized. The catalytic property of Bi₂WO₆/graphene composited aerogel has been investigated [16]. However, to the best of our knowledge, Bi₂WO₆/graphene hybrid aerogel as capacitor electrodes has not been reported.

In this research, we report a simple method to synthesize a unique 3D Bi₂WO₆-graphene hybrid aerogel (BWGA) as an active electrocatalyst for supercapacitor electrode. Benefiting from its poriferous architectures, large specific area, and excellent electroconductibility, the BWGA composites exhibit excellent rate capability, higher specific capacitance, and larger energy density.

Experimental

Synthesis of Bi₂WO₆ nanosheets

All the reagents used were analytic grade reagents and used without further purification. Experiment details were as follows: 0.97 g Bi(NO₃)₂•5H₂O was put into 40 mL of nitric acid solution (1 mol L⁻¹). A transparent aqueous solution was formed after sonication for 30 min. The solution was marked as solution A. In the meantime, 0.23g Na₂WO₄•2H₂O and 0.05g cetyl-trimethyl

ammonium bromide were put into 40 mL deionized water to form the solution. The obtained solution was marked as solution B. Then solution B was added into A rapidly under drastic stirring for 30 min. Then the pH value of the mixed solution was controlled to about 7.5 by ethylenediamine. The obtained mixed solution was consequently added into a Teflon-lined autoclave. Then the autoclave was sealed and heated at 120 °C for 24 h. After the heating reaction, the ivory product was then collected by centrifugal separation. Then the product was washed by de-ionized water and absolute ethanol to remove any residual. Then the Bi₂WO₆ nanosheets were obtained after freeze-dried for 24 h.

Preparation of graphene oxide (GO)

In a typical synthesis process, 9:1 mixture of concentrated H₂SO₄/H₃PO₄ (180/20 mL) solution was added to a 250 mL flask containing 1.5 g of graphite and 4.5 g of KMnO₄ at low temperature (0-5 °C). Then the flask was heated to 50 °C in an oil-bath for 15 h. After that, 150 g ice was added into the resulting suspension to dilute the solution and 2 mL H₂O₂ (30 wt%) was injected. Then the reaction product was washed twice by 100 mL HCl (10 wt%). The remaining GO suspension was washed several times until the pH of GO suspension was above 6. Then the GO suspension was freeze-dried to obtain the final product.

Synthesis of BWGA composites

The BWGA composites were prepared by a self-assembly process. A typical procedure is as following: 10 mg of GO powders were added into the 10 mL deionized water. An orange transparent solution was got after sonication for 60 min. Then 90 mg of Bi₂WO₆ nanosheets were put into the solution. A homogeneous suspension was obtained after sonication. Then 50 µL ethylenediamine was put into the suspension. The obtained solution was consequently added into a Teflon-lined autoclave after stirring for 30 min. Then the autoclave was sealed and heated at 120 °C for 10 h. After the heating reaction, the black jellylike hydrogel was then collected and washed by de-ionized water to eliminate any residual. Then the hydrogel was freeze-dried for 48 h to get BWGA composites.

Characterizations

X-ray diffraction (XRD) of all the prepared materials were performed on a Rigaku Ultima IV diffraction instrument (Rigaku Co., Japan) using a Cu tube as X-ray source ($\lambda_{\text{Cu K}\alpha} = 1.54 \text{ \AA}$), a tube voltage of 35 kV and a current of 35 mA. The morphologies of the samples were characterized by scanning electronic microscopy (SEM) using a Zeiss SIGMA microscope (Carl Zeiss Co., Germany) and transmission electron microscope (TEM) using a Tecnai F30 microscope (FEI Co., US). Quantachrome instruments Quadrasorb SI (US) was used to measure the Brunauer-Emmett-Teller (BET) surface areas of the samples at liquid nitrogen temperature (77.3K).

Electrochemical measurements

The working electrodes were fabricated by mixing the sample (80 wt%) with 10 wt% acetylene black and 10 wt% polytetrafluorene-ethylene (PTFE) binder. The obtained mixture gelatinoid was coated on to Ni foam (1.0 cm x 1.0 cm), followed by dried in drying oven overnight at 60 °C. The loading mass on the Ni foam is about 3-5 mg cm⁻². Electrochemical measurement was carried out in a conventional three-electrode cell with 6 M KOH as the electrolyte. Platinum foil and Ag/AgCl electrode were used as the counter and reference electrodes, respectively. Cyclic voltammetry (CV), Charge and discharge measurements and electrochemical impedance spectroscopy (EIS) were performed with a CHI 660C electrochemical workstation (Shanghai Chenhua, China).

Results and discussion

Fig. 1a presents the X-ray diffraction (XRD) patterns of Bi₂WO₆ and BWGA. The diffraction peaks at 27.9°, 32.8°, 47.2°, 55.8°, 58.5° and 75.7° can be indexed to (1 3 1), (2 0 0), (2 0 2), (1 3 3), (2 6 2), and (4 0 0) crystal planes of bismuth tungstate phase (JCPDS no.39-0256), respectively. No other impurity peak is found which indicate that the hydrothermal synthesis process occurred completely. The swell band at about 25° for the composites can be indexed to the (002) crystal planes of graphite which verify that the GO in the BWGA has been reduced to the graphene [16, 17]. The Raman modes (**Fig. 1b**) in the range of 790-830 cm⁻¹ can be indexed to the symmetric and asymmetric stretching modes of the WO₆ octahedra. The bands at around 180-500 cm⁻¹ region can be ascribed to the bending modes of the WO₆ octahedra coupled with stretching and bending modes of the Bi-O polyhedron. The modes below 200 cm⁻¹ can be indexed to the chemical link of the W and Bi ions [18, 19]. The Raman spectrum (**Fig. 1b**) of BWGA shows two characteristic bands at 1350 and 1650 cm⁻¹, which can be indexed to the D and G band of graphene, respectively [20]. The analysis results of Raman spectra also confirm that the BWGA is composed of Bi₂WO₆ and graphene.

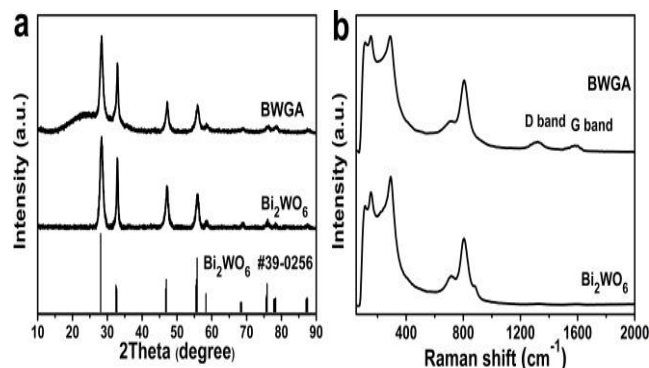


Fig. 1. (a) XRD pattern and (b) Raman spectra of the Bi₂WO₆ nanosheets and BWGA.

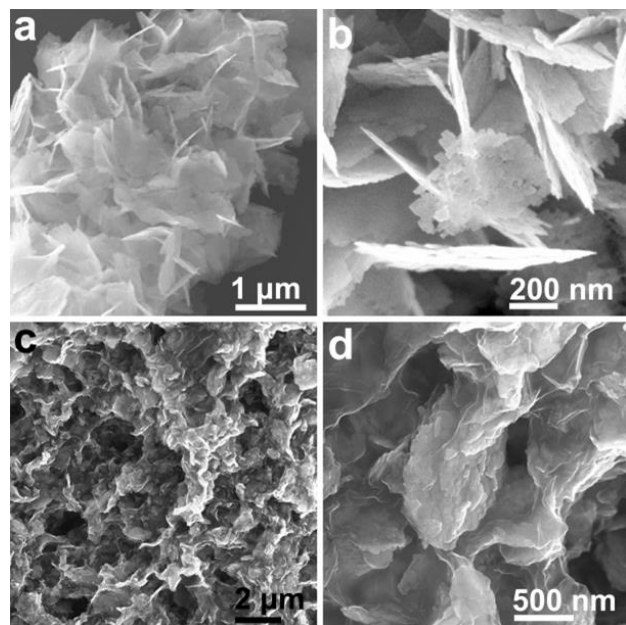


Fig. 2. FESEM images of Bi_2WO_6 ((a), (b)) and BWGA ((c), (d)).

Typical morphology of the product is investigated by FESEM and TEM. The morphology and structure of the Bi_2WO_6 nanosheets are shown in Fig. 2a. It could be found that the Bi_2WO_6 samples are almost flake-like structure, indicating the high yield and excellent uniformity of Bi_2WO_6 nanosheets. Magnification FESEM image of Bi_2WO_6 is shown in Fig. 2b and the image obviously reveals that the as-prepared Bi_2WO_6 are flake like structure with the average shape of $\sim 1 \mu\text{m}$ and the thickness of $\sim 20 \text{ nm}$. The structure and morphology details of the Bi_2WO_6 nanosheets are further detected by TEM. TEM image (Fig. S1) reveals that the flake-like Bi_2WO_6 is consisted of micro Bi_2WO_6 particles with the average diameter of $\sim 50 \text{ nm}$. FESEM images of BWGA are shown in Fig. 2c-d. The FESEM images exhibit an interconnected and polyporous 3D framework formed by graphene and Bi_2WO_6 nanosheets. The pore structure in the framework is highly continuous and the mean sizes of these pores are about $1 \mu\text{m}$. As shown in the enlarged drawing of BWGA (Fig. 2d), it is noteworthy that Bi_2WO_6 nanosheets and graphene are closely stacked in the framework structure of BWGA and most of the Bi_2WO_6 nanosheets are wrapped in graphene sheets.

Brunauer Emmett Teller (BET) curves are shown in Fig. 3. The specific surface area of BWGA composite is $39.4 \text{ m}^2 \text{ g}^{-1}$ based on the test (Fig. 3a). The specific area is about 60% larger than that of Bi_2WO_6 nanosheets ($24.1 \text{ m}^2 \text{ g}^{-1}$). The increase of the surface area could possibly be ascribed to the interconnected and polyporous structure of hybrid composites. The specific construction of BWGA, high specific surface area, porous construction, and consecutive electrically conductive network not only reduce the agglomeration of Bi_2WO_6 nanosheets, but also supply abundant exposed active sites, which could improve the capacitance indirectly [21, 22].

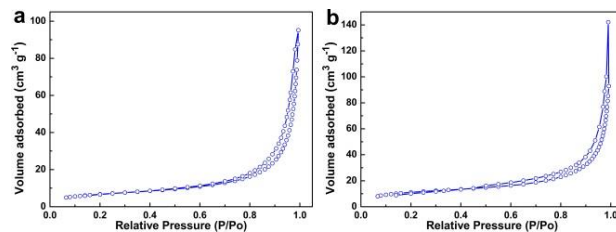


Fig. 3. N_2 adsorption isotherm of the Bi_2WO_6 nanosheets (a), BWGA (b).

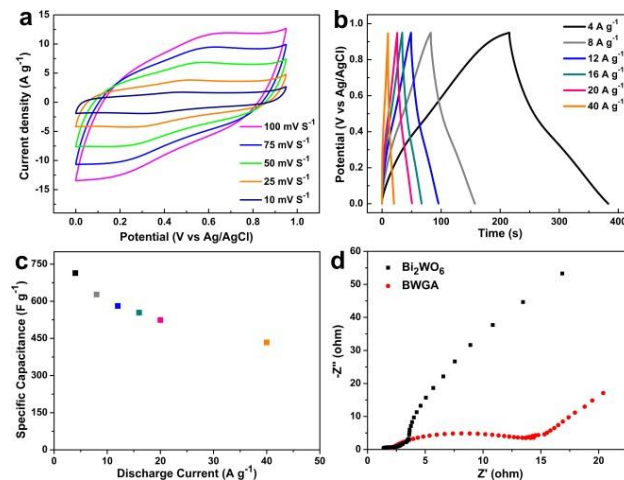


Fig. 4. Electrochemical properties of the BWGA electrodes. (a) Typical cyclic voltammetry (CV) curves at various scan rates of 10, 25, 50, 75, and 100 mV s^{-1} , (b) Galvanostatic charge/discharge curves of BWGA at different current densities of 4, 8, 12, 16, 20, and 40 A g^{-1} , (c) Specific capacitances at different current densities, (d) Nyquist plots of Bi_2WO_6 and BWGA electrodes.

Typical cyclic voltammetry (CV) curves of the BWGA composite electrode at various scan rates are shown in Fig. 4a. At lower scan rates of 10 and 25 mV s^{-1} , a pair of redox peaks could be found clearly in the CV curves. The characteristics of CV curves and the redox peaks are mainly related to the reduction-oxidation reactions of bismuth tungstate happened during the CV process [13]. Fig. 4b shows the charge/discharge curves of the BWGA composites electrode at various current densities in the operating voltage range of 0-0.95 V. The specific capacitance values are calculated (base on the mass of BWGA) to be approximately 714, 627, 581, 554, 524, and 434 F g^{-1} at 4, 8, 12, 16, 20, and 40 A g^{-1} (Fig. 4c), respectively, which are larger than those of other Bismuth-based materials (Table S1) [10-13]. As shown in the Fig. 4c, the specific capacitance of the electrode is slightly dropped when the operating current density is increased. The results indicate the good rate performance of BWGA electrode due to the introduction of graphene matrix which works as a conductive network [13, 23]. The good electroconductibility of BWGA composite can be verified by the electrochemical impedance spectroscopy (EIS) test. As shown in Fig. 4d, the BWGA electrode exhibits a smaller frequency semicircle than the Bi_2WO_6 material, indicating the better electroconductibility due to the composite of conductive graphene framework. [24].

Conclusion

In summary, we have developed a simple method to synthesis the 3D porous Bi₂WO₆/graphene hybrid aerogel. In this Bi₂WO₆/graphene hybrid aerogel, a 3D conductive graphene framework is formed as a charge transfer pathway, which contributes to the high specific capacitance. The 3D BWGA composite could provide a new prospect for design and synthesis of high-performance and low-cost materials for rechargeable energy-storage devices.

Acknowledgements

The authors would like to thank the National Natural Science Foundation of China (51372212).

Author's contributions

Conceived the plan: zcw; Performed the experiments: xx, jqh; Data analysis: xx, fwm; Wrote the paper: xx, zcw. Authors have no competing financial interests.

Supporting information

Supporting informations are available from VBRI Press.

References

1. Winter, M.; Brodd, R. J.; *Chem. Rev.*, **2004**, *104*, 4245–4270.
DOI: [10.1021/cr020730k](https://doi.org/10.1021/cr020730k)
2. Aricò, A. S.; Bruce, P.; Scrosati, B.; Tarascon, J. M.; Van Schalkwijk, W.; *Nat. Mater.*, **2005**, *4*, 366–377.
DOI: [10.1038/nmat1368](https://doi.org/10.1038/nmat1368)
3. Peng, Z.; Liu, Y.; Chen, K.; Yang, G.; Chen, W.; *Chem. Eng. J.*, **2014**, *244*, 335–342.
DOI: [10.1016/j.cej.2014.01.053](https://doi.org/10.1016/j.cej.2014.01.053)
4. Peng, Z.; Liu, Y.; Zhao, Y.; Shu, Wei.; Chen, K.; Bao, Q.; Chen, Wen.; *Electrochim. Acta*, **2013**, *111*, 755–761.
DOI: [10.1016/j.cej.2015.07.049](https://doi.org/10.1016/j.cej.2015.07.049)
5. Simon, P.; Gogotsi Y., Dunn; B.; *Science*, **2014**, *343*, 1210–1211;
DOI: [10.1126/science.1249625](https://doi.org/10.1126/science.1249625)
6. Simon, P.; Gogotsi, Y.; *Nat. Mater.*, **2008**, *7*, 845–854.
DOI: [10.1038/nmat2297](https://doi.org/10.1038/nmat2297)
7. Sha, C.; Lu, B.; Mao, H.; Cheng, J.; Pan, X.; Lu, J.; Ye, Z.; *Carbon*, **2016**, *99*, 26–34.
DOI: [10.1016/j.carbon.2015.11.066](https://doi.org/10.1016/j.carbon.2015.11.066)
8. Yang, X.; Cheng, C.; Wang, Y.; Qiu, L.; Li, D.; *Science.*, **2013**, *341*, 534–537.
DOI: [10.1126/science.1239089](https://doi.org/10.1126/science.1239089)
9. Jung, N.; Kwon, S.; Lee, D.; Yoon, D.-M.; Park, Y. M.; Benayad, A.; Choi, J.-Y.; Park, J. S.; *Adv. Mater.*, **2013**, *25*, 6854–6858.
DOI: [10.1002/adma.201302788](https://doi.org/10.1002/adma.201302788)
10. Patil, S.S.; Dubal, D.P.; Tamboli, M.S.; Ambekar, J. D.; Kolekar, S. S.; Gomez-Romero, P.; Kale, B.B.; Patil, D.R.; *J. Mater. Chem. A*, **2016**, *4*, 7580–7584.
DOI: [10.1039/c6ta01980c](https://doi.org/10.1039/c6ta01980c)
11. Huang, X.; Zhang, W.; Tang, Y.; Wu, J.; Gao, Y.; Tang, B.; *Ceram. Int.*, **2016**, *42*, 2099–2105.
DOI: [10.1016/j.ceramint.2015.09.157](https://doi.org/10.1016/j.ceramint.2015.09.157)
12. Khan, Z.; Bhattu, S.; Haram, S.; Khushalani, D.; *RSC Adv.*, **2014**, *4*, 17378–17381.
DOI: [10.3365/eml.2009.06.087](https://doi.org/10.3365/eml.2009.06.087)
13. Nithya, V.D.; Kalai Selvan, R.; Kalpana, D.; Vasylechko, C.; Sanjeeviraja, C.; *Electrochim. Acta*, **2013**, *109*, 720–731.
DOI: [10.1016/j.electacta.2013.07.138](https://doi.org/10.1016/j.electacta.2013.07.138)
14. Sha, C.; Lu, B.; Mao, H.; Cheng, J.; Pang, X.; Lu, J.; *Carbon*, **2016**, *99*, 26–34.
DOI: [10.1016/j.carbon.2015.11.066](https://doi.org/10.1016/j.carbon.2015.11.066)
15. Mao, Lu.; Guan, C.; Huang, X.; Ke, Q.; Zhang, Y.; Wang, J.; *Electrochim. Acta*, **2016**, *196*, 653–660.
DOI: [10.1016/j.electacta.2016.02.084](https://doi.org/10.1016/j.electacta.2016.02.084)
16. Xu, X.; Ming, F.; Hong, J.; Xie, Y.; Wang, Z.; *Mater. Letts.*, **2016**, *179*, 52–56.
DOI: [10.1016/j.matlet.2016.05.031](https://doi.org/10.1016/j.matlet.2016.05.031)
17. Xu, Y.; Bai, H.; Lu, G.; Li, C.; Shi, G.; *J. Am. Chem. Soc.*, **2008**, *130*, 5856–5857.
DOI: [10.1021/ja800745y](https://doi.org/10.1021/ja800745y)
18. Maczka, M.; Fuentes, A. F.; Kepinski, L.; Diaz-Guillen, M. R.; Hanuza, J.; *Mater. Chem. Phys.*, **2010**, *120*, 289–295.
DOI: [10.1016/j.matchemphys.2009.11.006](https://doi.org/10.1016/j.matchemphys.2009.11.006)
19. Maczka, M.; Macalik, L.; Hermanowicz, K.; Kępiński, L.; Tomaszewski, P.; *J. Raman. Spectrosc.*, **2010**, *41*, 1059–1066.
DOI: [10.1002/jrs.2526](https://doi.org/10.1002/jrs.2526)
20. Zheng, Q.; Cai, Z.; Ma, Z.; Gong, S.; *ACS Appl. Mater. Interfaces*, **2015**, *7*, 3263–3271.
DOI: [10.1021/am507999s](https://doi.org/10.1021/am507999s)
21. Cao, X.; Zheng, B.; Rui, X.; hi, W.; Yan, Q.; Zhang, H.; *Angew. Chem. Int. Ed.*, **2014**, *53*, 1404–1409.
DOI: [10.1002/anie.201308013](https://doi.org/10.1002/anie.201308013)
22. Cao, X.; Shi, Y.; hi, W.; Lu, G.; Huang, X.; Yan, Q.; Zhang, Q.; Zhang, H.; *Small*, **2011**, *7*, 3163–3168.
DOI: [10.1002/sml.201100990](https://doi.org/10.1002/sml.201100990)
23. Wang, Q.; Liu, B.; Wang, X.; Ran, S.; Wang, L.; Chen, D.; Shen, G.; *J. Mater. Chem.*, **2012**, *22*, 21647–21653.
DOI: [10.1039/C2JM34705A](https://doi.org/10.1039/C2JM34705A)
24. Qu, Q.; Zhang, P.; Wang, B.; Chen, Y.; Tian, S.; Wu, Y.; Holze, R.; *J. Phys Chem C.*, **2009**, *113*, 14020–14027.
DOI: [10.1021/jp8113094](https://doi.org/10.1021/jp8113094)